Journal of Mining and Environment (JME) Published online

Shahrood University of Technology

Journal of Mining and Environment (JME)

Journal homepage: www.jme.shahroodut.ac.ir

Iranian Society of Mining Engineering (IRSME)

An Approach for Estimation of Uniaxial Compressive Strength and Internal Friction Angle using Well Log Data and Deep Learning Algorithms

Farhad Mollaei, Ali Moradzadeh*, and Reza Mohebian

School of Mining, College of Engineering, University of Tehran, Tehran, Iran

Article Info

Received 1 September 2024

Received in Revised form 4 December 2024

Accepted 9 December 2024

Published online 9 December 2024

DOI: 10.22044/jme.2024.15006.2859

Keywords

Mechanical parameters

Log data

DL models

Core data

Feature selection

Abstract

The important aspects of this study are to estimate the mechanical parameters of reservoir rock including Uniaxial Compressive Strength (UCS) and friction (FR) angle using well log data. The aim of this research is to estimate the UCS and FR angle (φ) using new deep learning (DL) methods including Multi-Layer Perceptron (MLP), Long Short-Term Memory (LSTM), Convolutional Neural Network (CNN), and CNN + LSTM (CL) by well log and core test data of one Iranian hydrocarbon field. As only 12 UCS and 6 FR core tests of single well in this field were available, they were firstly calculated, and then generalized to other depths using two newly derived equations and relevant logs. Next, the effective input logs' data for predicting these parameters have been selected by an auto-encoder DL method, and finally, the values of UCS and φ angle were predicted by the MLP, LSTM, CNN, and CL networks. The efficiency of these four prediction models was then evaluated using a blind dataset, and a range of statistical measures applied to training, testing, and blind datasets. Results show that all four models achieve satisfactory prediction accuracy. However, the CL model outperformed the others, yielding the lowest RMSE of 1.0052 and the highest R^2 of 0.9983 for UCS prediction, along with an RMSE of 0.0201 and R^2 of 0.9917 for φ angle prediction on the blind dataset. These findings highlight the high accuracy of deep learning algorithms, particularly the CL algorithm, which demonstrates superior precision compared to the MLP method.

1. Introduction

Reservoir studies are a major part of reservoir management. One of the important aspects of this study is to estimate two important geomechanical parameters of reservoir rock including Uniaxial Compressive Strength (UCS) and friction angle. These are of the most practical geomechanical and engineering parameters, which is an urgent requirement for petroleum engineers in most designs and modeling related to the wellbore stability, creating Earth Geomechanical Model (EGM), reservoir depletion, and its cap rock integrity, and hydraulic fracturing projects. Compressive strength is the bearing capacity of an object, building material or structure against compressive forces. When the compressive strength of a material is reached, that material will be destroyed. Usually, the UCS of rock samples is determined by using the UCS test in the laboratory. In this experiment, the strain of the rock sample is measured by increasing the uniaxial compressive force. The stress at the moment of failure is considered as the maximum resistance of the rock. Another method for predicting UCS is to use index tests (such as point load test). Determining the uniaxial compressive strength in the laboratory requires core samples of appropriate quality, which are time-consuming and expensive to prepare based on the necessary standards. On the other hand, the results of the laboratory values also strongly depend on the dimensions of the sample, loading, human errors and other external factors. Furthermore, due to the impossibility of preparing suitable samples from weak, broken and crushed rocks, indirect estimation of UCS seems necessary

Corresponding author: a_moradzadeh@ut.ac.ir (A. Moradzadeh)

in most practical cases. Friction angle (φ) is the angle at which a rock unit can tolerate shear stress.

The principles of UCS estimation are usually done by using statistical methods such as simple linear regression, non-linear multiple regression or by experimental methods for indirect estimation. Some of these studies are mentioned below: Cargill and Shakoor (1990), provided a relationship between UCS value with parameters such as Schmidt hammer (Rn) and point load index. The results showed that there is a strong correlation between point load index and UCS [1]. Tuğrul and Zarif (1999) proposed a simple regression analysis to obtain relationships between UCS and other rock properties including p wave velocity (Vp), point load index, and tensile strength using Brazilian test [2]. Karakus and Tutmez (2006) used a multi-variate regression model to present a relationship for estimating UCS based on several parameters that the parameters were such as return values of Schmidt's hammer (Rn), point load index, and p wave velocity (Vp) [3]. Yagiz (2011), estimated the UCS by non-destructive testing using parameters of Schmidt hardness (Rn), p wave velocity (Vp), effective porosity and dry density [4]. Singh et al. (2013), proposed an experimental relationship between the point load index and UCS for some Indian rocks [5]. Aladejare (2020) used experimental models to estimate UCS. He used the data of return values of Schmidt hammer (Rn), point load index, block punch index (BPI), effective porosity, and density as input for experimental estimation of UCS. Then he compared the estimated values of UCS obtained from experimental equations with regression methods and concluded that experimental methods are less accurate than regression methods due to the different behavior of rocks in each region [6].

In addition, in recent years, various researchers used artificial intelligence (AI) methods to estimate geomechanical parameters (e.g. Hazbeh et al. (2024), predicted shear wave velocity [7], Mollaei et al. (2024), predicted brittleness index [8], Mollaei et al. (2024) estimated shear wave velocity [9], and etc.) and UCS using parameters such as point load index, p-wave velocity, and Schmidt hammer hardness using core test dataset, which some of the most important them are mentioned here. Gokceoglu (2002) presented a fuzzy triangular diagram to predict the uniaxial compressive strength of Ankara agglomerates from their lithological composition. He used the values account for VAF, variance calculation, and RMSE calculation to control the performance of triangle prediction capacity, which achieved good results [10]. Yılmaz, and Yuksek (2008) predicted the UCS using Artificial Neural Network (ANN). They predicted UCS and elastic modulus using Multiple Regression (MR), ANN, and Adaptive Neural Fuzzy Inference System (ANFIS) models [11]. Tiryaki (2008) presented a method to predict the strength of healthy rock for mechanical drilling using multi-variate statistics, ANN, and regression trees. He used bivariate correlation and curve fitting tests to estimate the UCS for the rocks [12]. Sarkar et al. (2010) used artificial neural network method to predict the UCS with the input parameters of dynamic wave velocity, durability index, p-wave velocity, and density [13]. Dehghan et al. (2010) predicted the UCS and elastic modulus using regression and ANNs [14]. Manouchehrian et al. (2012), investigated the usage of ANN and multivariate statistics to estimate the UCS using textural characteristics of rock [15]. Rabbani et al. (2012) predicted the UCS by artificial neural network [16]. Singh and Verma (2012) used an intelligent algorithm to correlate UCS with parameters such as porosity, tensile strength, and point load index in schistose rocks [17]. Yesiloglu-Gultekin et al. (2013) presented research entitled predicting the UCS of granite by different non-linear tools, and comparing their performance, in which three different methods of multi-variate regression analysis, ANN, and ANFIS were used to estimate this parameter [18]. Majdi and Rezaei (2013) used an artificial neural network and Multi-Variable Regression Analysis (MVRA) models in order to predict UCS of rock surrounding a roadway using 93 laboratory datasets. The UCS estimation was based on the rock type, Schmidt hardness, density and porosity as input parameters [19]. Mishra and Basu (2013) estimated UCS using Regression Analysis (RA) and Fuzzy Inference System (FIS) [20]. Rezaei et al. (2014) predicted the UCS using fuzzy logic [21]. Mohamad et al. (2015) predicted the UCS using a hybrid particle swarm optimization (PSO)-based ANN model and 160 laboratory test data [22]. Armaqhandi et al. (2018) estimated the UCS of rock on 20 sandstone samples in Malaysia by using the Gene Expression Programming (GEP) algorithm. In this research, in order to show the capability of this algorithm, the model was compared with linear regression, and the results showed that the GEP model is more accurate for estimating UCS [23]. To predict UCS, Saeedi et al. (2018) used input parameters including Brazilian Tensile Strength (BSI), point load index, and P-wave velocity across various rock types. In their study, they applied multiple regression analysis, ANN, and ANFIS to predict

UCS. The findings indicated that the multiple regression approach was less accurate than both the artificial neural network and the adaptive neuro-fuzzy inference system [24]. Rezaei and Asadizadeh (2020) employed a combination of intelligent techniques including ANFIS, genetic algorithm (GA), and PSO, to predict rock UCS. These models were developed using laboratory datasets from 93 core samples, spanning a range of rock strengths from weak to very strong [25]. Rezaei and Asadizadeh (2020) use the new combinations of intelligent techniques including ANFIS, genetic algorithm (GA), and PSO in order to predict rock UCS. These models were constructed based on the collected laboratory datasets upon 93 core specimens ranging from weak to very strong rock types. They concluded the ANFIS-GA model was more accurate than the PSO-based ANFIS and MR models [25]. Wang and Wen (2019) estimated the UCS with the GEP algorithm using the return values of the Schmidt hammer (as an input parameter) [26]. Fattahi (2020) predicted the UCS with Relevance Vector Regression (RVR), improved by the Cuckoo Search (CS) and Harmony Search (HS) algorithms that introduced to forecast UCSWR. The HS and CS algorithms are combined with RVR to determine the optimal values for the RVR controlling factors [27]. Hassan and Arman (2022) estimated the UCS of carbonate rock by using a simple, measured Schmidt Hammer (SHV_C) test on core sample and a unit weight (γ_n) of carbonate rock [28]. Dadhich et al. (2022) used machine learning (ML) algorithms to estimate the uniaxial compressive strength of rock using point load strength, porosity, Schmidt rebound hardness, block punch index, and specific gravity [29]. Afolagboye et al. (2023) used four ML models of; Random Forest (RF), Relevance Vector Machine (RVM), Support Vector Machine (SVM), and ANN to predict the UCS values of Precambrian basement rocks [30]. Ibrahim et al. (2024) estimated uniaxial compressive strength (UCS) and tensile strength (T0) using random forest (RF) and decision tree (DT) models, based on well-logging data from a Middle Eastern reservoir [31].

Additionally, only a few researchers have concentrated on predicting the φ angle and cohesion of soil samples using ML methods. Among them, Allush et al. (2017) predicted rocks' uniaxial compressive strength and rock's φ angle using ML algorithms such as ANFIS, SVM, and ANN [32]. Pham et al. (2021) estimated the soil's φ angle using 245 laboratory test data points and a deep neural network (DNN) optimized with a PSO algorithm [33]. Hiba et al. (2022) predicted friction angle and adhesion using well log data and machine learning algorithms including RF and DT [34]. Faraj et al. (2022) estimated FR angle with density and gamma neutron logs using Plumb's correlation [35]. Shahani et al. (2022) estimated φ angle and adhesion using ML method (Lasso regression (LR), ridge regression (RR), decision tree (DT), and SVM and logs data [36]. Ngoyan et al. (2024) utilized Bayesian backpropagation regularization algorithm to predict soil's φ angle [37].

As stated previously, most studies conducted for this purpose have utilized various intelligent methods, primarily based on laboratory test data from rock and occasionally soil samples. Given that such data are often unavailable for geomechanical studies of hydrocarbon reservoirs, it is essential to estimate the values of these important geomechanical parameters across the entire reservoir interval or its wells using well log data and more advanced, powerful deep learning methods. As accurate estimation of these parameters is very important for modeling and geomechanical studies; this study try to introduce methods for estimating these parameters using deep learning algorithms and well log data with high accuracy, and low-cost continuously. On this basis, here four algorithms of MLP, CNN, LSTM, and CL are used to predict UCS and φ angle. To achieve the goal, a set of well logs and core data was chosen from a vertical well in one of the hydrocarbon fields in southern part of Iran. In the first step, one type of Auto-encoders deep network was used to select the effective features related to these parameters. Subsequently, the selected logs were utilized as input parameters of the model to predict the UCS and φ angle using four MLP, LSTM, CNN, and CL algorithms. Finally, the performance of these four algorithms have been evaluated using a blind dataset, and their results compared with each other using various statistical measures. This study marks the first use of the Auto-encoder algorithm for feature selection. It is also the first time a hybrid DL approach, known as CL, is utilized alongside with other deep learning models to predict rock's φ angle and UCS values along the entire well path using selected well log data. Moreover, there is a noticeable gap in the literature regarding the estimation of rocks' φ angle with DL methods, especially using hybrid models like CNN + LSTM (CL). This underscores the essential need for further research in this area.

2. Material and Methods
2.1. Methods
2.1.1. Multi-layer perceptron neural network

A Multi-Layer Perceptron (MLP) neural network will be obtained by stacking several perceptron. In such a network, we will have several layers of neurons. Figure 1 shows an example of a MLP neural network: the first layer is known as the input layer. The data is transferred sequentially through one or more intermediate (or hidden) layers. At each layer, the data undergoes a series of mathematical transformations, which, gradually extract and refine features. Ultimately, the transformed data reaches the output layer, where the network produces its final output based on the learned patterns in the data [38].

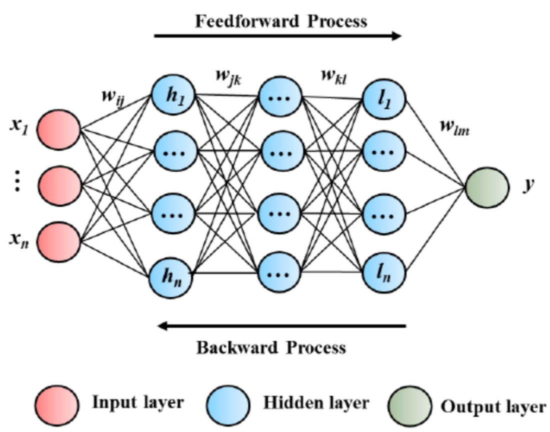

Figure 1. Schematic of an MLP neural network structure [39].

The MLP network employs two: the feedforward propagation and backpropagation training methods. In the first training process, input feature nodes (neurons) are multiplied by corresponding weights and biases to produce output values that pass through non-linear activation functions across all hidden layers. Backpropagation, on the other hand, adjusts these weights to minimize loss by applying gradient descent after predicting the target and computing the loss in the forward pass. In an MLP, each layer's output becomes the input for the subsequent layer, establishing a layered architecture that processes data progressively from the primary input layer through hidden layers to the output layer. The network's adjustable weights are the core of this process: they are applied to the connections between neurons and adjusted based on the desired classification or clustering outcome of the network. These weights are dynamically adjusted during the training process through backpropagation, an algorithm that minimizes error by fine-tuning weights in response to the network's performance. As the data is passed through each node, it is also processed by an activation function. This function introduces non-linearities, which allow the MLP to model complex relationships within the data that linear functions alone could not capture. Examples of commonly used activation functions include the sigmoid, Rectified Linear Unit (ReLU), and tanh functions, each offering unique benefits for handling various data patterns. The combination of weights, activation functions, and layer connections forms the basis of the MLP's machine learning process. According to Figure 1, the training process of an MLP neural network is illustrated by the following equation: [39].

$$y_m = f(\sum_{i}^{m} w_l\, m y_l + w_m) \tag{1}$$

Here, y_m represents the predicted value at the mth output layer, y_l denotes output of the lth hidden layer, w_{lm} is the weight connecting the lth hidden layer to the mth output layer, w_m indicates the weight at the mth output layer, f is the activation function, i is the input layer, and m is the output layer.

2.1.2. Recurrent neural networks

Recurrent Neural Networks (RNNs) are a powerful type of deep learning network, particularly useful for sequential data such as time series. One of the main problems of RNN is gradient vanishing when learning from long-term sequences, which reduces the learning ability of the algorithm. In fact, simple RNNs cannot learn long-term sequences, and this problem led to the creation of recurrent neural networks with long short-term memory (LSTM). LSTM networks are a type of RNN designed with specific modifications that enable them to capture long-term dependencies and effectively manage long-term memory. The key difference between an LSTM and a traditional RNN lies in the structure of the LSTM unit, which includes additional components specifically engineered to handle the vanishing gradient problem. This structure allows LSTMs to selectively remember or forget information over extended sequences, making them highly effective for tasks that require memory retention over long periods. In one LSTM block we have three inputs (x, h and c). x is the input at time (sequence) t, and h, like simple RNN, is the "hidden state" that receives from the output of the previous time (previous sequence) as memory. The input c is a "cell state" that controls how much information from the previous long sequences and which ones are affected in the block. Any LSTM block can be divided into three main parts [39]. In Figure 2, part (1) is called the forget gate. This part of the block decides which part of the previous long information (past long sequences) is useful in the current block and which part is not. In this part, "current input (x)" and "previous hidden state (h)" are combined (by weights) and given to the sigmoid activation function, and then the output is multiplied by "cell state (c)". In this part, the learning is done by the weights of a small internal neural network, when combining x and h, so that they can adjust their multiplication c. Section (2): This section decides what new information should be added to "Cell State (c)" for later use. This part, which is called "input gate", is made by combining "current input (x)" and "previous hidden state (h)" and combining it by the weights of small internal neural networks with the output of the previous part (forget gate). In section (3) in Figure (3), there is an "output port" that specifies the outputs. These outputs are a combination of "cell state (c) that has been updated" combined with "current input (x)" and "previously hidden state (h)". At this stage, there is also an internal neural network for learning. The outputs h and c are used in the next time (t+1), that is, in the next sequence of the same example.

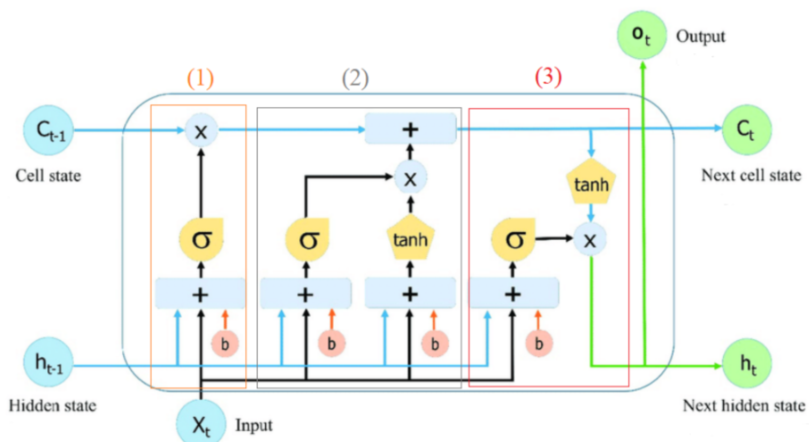

Figure 2. Structure of an LSTM block [41].

In summary, LSTMs improve upon traditional RNNs by incorporating memory-management mechanisms through the forget, input, and output gates. These components work together to balance long-term and short-term memory within the network, enabling LSTMs to capture dependencies over extended time steps without encountering the vanishing gradient problem. By retaining and updating relevant information across sequences, LSTMs are highly effective in tasks that require an understanding of long-term contextual information, such as time-series forecasting.

2.1.3. Convolutional neural network

Convolutional Neural Networks (CNNs) are among the most powerful deep learning methods. CNNs leverage a series of specialized layers that are trained to automatically extract and learn hierarchical features from data, producing highly accurate models for image classification, object detection, and more [42]. Figure 3 illustrates a typical CNN architecture, which consists of three main types of layers: the convolutional layer, pooling layer, and fully connected layer. Each layer performs a unique function, contributing to the network's ability to learn complex patterns. In CNNs, training typically involves two main stages: the feed-forward stage and the backpropagation stage. In the first stage, the input data is fed through the network and each neuron performs a point-wise multiplication between its parameters (or weights) and the input data. This process, known as the convolution operation, extracts feature from the input data at various levels of abstraction. The final output of the feed-forward stage is the predicted result, which is subsequently used to compute the network error. This error is calculated by comparing the network's output to the true label using an error function or loss function (e.g. mean squared error or cross-entropy loss). Once the error is determined, the network begins the second (backpropagation) stage to optimize its parameters. The gradient of the error is then calculated with respect to each parameter using the chain rule, and each parameter is adjusted based on its contribution to the total error. This iterative process—known as gradient descent—continues until the error reaches a minimum, allowing the network to learn and improve its accuracy with each pass. After each backpropagation pass, the feed-forward stage repeats, with updated parameters. Training completes once the network reaches a pre-defined number of iterations or the error falls below a threshold.

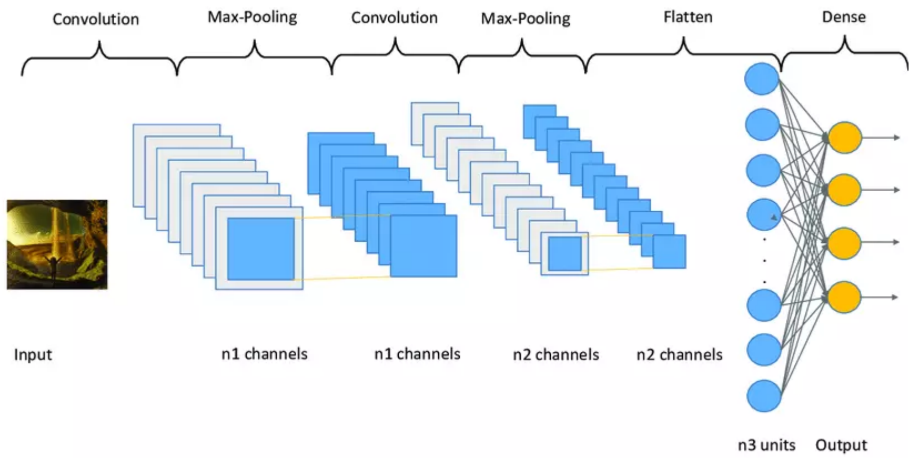

Figure 3. Schematic of CNN structure [42].

A CNN is structured as a hierarchical neural network, where convolutional layers are combined with pooling layers, followed by fully connected layers. Each of these layer types plays a distinct role: convolutional layers are the core feature extraction layers of a CNN. Each convolutional layer applies kernels (or filters) that convolve across the input image or preceding feature maps. The convolution operation emphasizes relevant patterns, such as edges, textures, or complex shapes, creating feature maps that represent learned aspects of the input data. As data passes through successive convolutional layers, these feature maps capture increasingly abstract patterns and structures within the data. Pooling layers typically follow convolutional layers and serve to down sample the feature maps, reducing their spatial dimensions. This reduction minimizes the number of parameters and computations within the network, helping control over fitting and enhancing computational efficiency. Common types of pooling include max pooling, which selects the maximum value within a region, and average pooling, which computes the average value. By retaining only the most significant information, pooling layers contribute to a more compact, resilient representation of features. After the final pooling layer, the feature maps are flattened into a 1D feature vector in preparation for the final classification or regression task. Fully connected layers then take this vector as input and further process it to produce the network's output. Each node in a fully connected layer connects to all activations in the previous layer, enabling the network to combine features and make more complex decisions based on the patterns it has learned [43].

2.2. Data presentation

The data of this research is related to one well of a hydrocarbon field in the southwest of Iran. This field is one of the largest oil fields in the Zagros basin, which is located in the eastern part of the structural area of Dezful embayment. This field is extended with a northwest-southeast trend in the western to central part and a northeast-southwest trend in the eastern part. The surface outcrop of this field is the Aghajari formation. The Asmari formation, the Bangestan and Khami groups are the hydrocarbon reservoirs in this field. Asmari formation is the most important reservoir rock of this field, which is divided into 6 reservoir layers. Reservoir layers one, two, three are mainly composed of dolomitic carbonates, so the density of fractures (especially in layer one) (90% dolomite) is higher. In the fourth, fifth and sixth reservoir layers of this field, due to the increase of shale and marl layers, as well as the decrease in fragility, the density of fractures decreases. The total available log data are 16330, which located in the depth range of 3551.072 to 3799.789 meters and 12 laboratory samples of UCS and, 6 laboratory samples of φ angle have been available. The available well logs include sum gamma ray (SGR), Corrected Gamma Ray (CGR), sonic travel time (DT), density (RHOB), resistivity (LL7), neutron porosity (NPHI), CALIPER, primary (P-wave) velocities (Vp), and the photoelectric factor (PEF). Table 1 presents a subset of these data logs, while Table 2 shows core sample data for uniaxial compressive strength and internal friction angle.

Table 1. Part of the available data logs.

DEPTH (m)	CALIPER (in)	CGR (GAPI)	SGR (GAPI)	Vp (m/s)	PEF (B/E)	LL7 (ohm.m)	RHOB (kg/m3)	NPHI (v/v)	DT (us/ft)
3551.682	9.602	5.656	28.5242	5644.444	3.4137	166.3624	2740	0.1	106
3551.834	9.6429	8.4385	31.2987	5750.943	3.4341	115.5674	2720	0.1	104
3551.987	9.7065	8.296	33.9424	5861.539	3.2612	64.433	2720	0.09	102
3552.139	9.6377	7.5697	35.947	5976.471	3.0593	40.084	2730	0.08	109
3552.292	9.5352	7.7178	37.2299	5976.471	3.0598	30.8807	2750	0.07	108
3552.444	9.5681	6.123	38.0726	5976.471	3.1447	26.2336	2770	0.06	109
3552.596	9.5648	4.4124	39.0551	5861.539	3.0769	26.9877	2780	0.06	110
3552.749	9.5716	3.0685	40.7509	5750.943	2.9428	32.131	2780	0.07	111
3552.901	9.5845	2.6307	43.2706	5750.943	2.806	34.8453	2780	0.08	113
3553.054	9.483	3.8246	46.2761	5644.444	2.7705	33.9128	2770	0.09	114
3553.206	9.4224	5.6863	49.3887	5644.444	2.7451	34.4455	2770	0.1	114
3553.358	9.414	6.3645	52.2282	5644.444	2.7313	33.7904	2760	0.1	114
3553.511	9.414	7.5808	54.713	5644.444	2.8674	32.8393	2750	0.1	113
3553.663	9.414	9.0363	57.1157	5750.943	3.0285	38.2476	2740	0.1	112
3553.816	9.4439	9.1963	59.8346	5861.539	3.0128	52.8836	2730	0.09	111

Table 2. Values of laboratory samples of UCS and φ angle.

Number	Depth (m)	laboratory UCS (Mpa)	laboratory φ (deg)
1	3553.054	90.052	43.89
2	3553.511	90.733	43.14
3	3555.644	80.518	40.96
4	3556.559	82.561	
5	3557.626	75.751	
6	3558.083	74.616	38.90
7	3558.997	89.825	42.40
8	3559.302	92.095	43.14
9	3560.216	92.549	
10	3560.826	90.96	
11	3561.588	85.512	
12	3562.655	88.236	

2.2.1. Feature selection

The relations between UCS and φ angle with conventional logs is a very complex nonlinear problem, which is the result of the interaction of many elements in the earth system, that makes it difficult for us to analyze and predict UCS and φ angle. Selecting the most sensitive logs, rather than utilizing all available conventional logs for model training and prediction, can decrease data processing requirements and enhance the model's speed and efficiency [44]. Moreover, feature selection also increases the prediction precision and universal applicability of the model. Therefore, in order to simplify the model structure, improve the modeling ability, enhance the model prediction efficiency, and alleviate the interference of the non-main parameter variables of the model to the prediction results, it is necessary to select the feature. So far, methods such as Pearson's or Spearman's correlation coefficient have been mainly used to select effective features. In this article, an Auto-encoder deep learning algorithm was employed as a novel approach for selecting the most relevant features for input data in four predictive: MLP, LSTM, CNN, and CL models. From the available log data—SGR, CGR, DT, RHOB, RT, NPHI, CALIPER, Vp, and PEF—the Auto-encoder algorithm identified four specific logs (Vp, RHOB, CALIPER, and NPHI) for UCS prediction. Similarly, it selected Vp, LL7 (RT), SGR, and NPHI as inputs for φ angle estimation. Figure 4 shows the process of feature selection using the above deep learning Auto-encoder code.

2.2.2. Data splits

Prediction reliability is one of the main concerns in the performance evaluation of supervised DL algorithms [40, 41]. Here, 16,330 well log data points were available within the depth range of 3551.072 to 3799.789 meters. Initially, 24% of these data points were set aside from the end of the dataset as blind data. From the remaining 12,330 data points, 80% were used as training data, while 20% served as test data. To prevent over fitting, a validation split of 0.1 was applied to the training dataset.

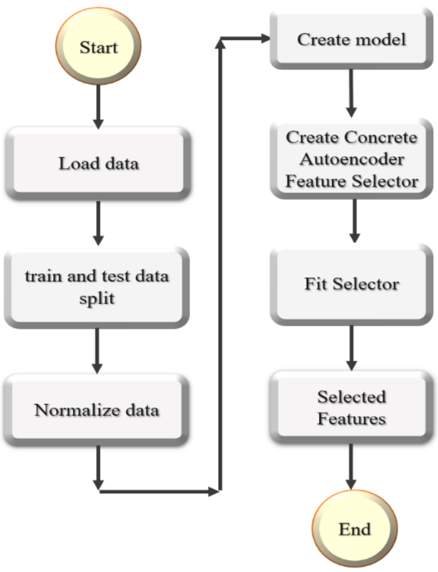

Figure 4. The workflow of feature selection using Auto-encoder algorithm.

2.2.3. Normalization

For reducing the prediction error from the difference of order of magnitude between the input data, the original data need to be preprocessed. Here, the Min-Max Normalization method was used to normalize the original data to [0,1] range, in order to eliminate the dimensional difference.

2.2.4. Optimization function

To optimize the algorithms, several optimizer functions—including Adam, Adamax, Nadam, RMSprop, Ftrl, SGD, and Adadelta—were evaluated. As shown in Figure 5, the Adam optimizer demonstrated the highest accuracy for estimating uniaxial compressive strength and internal friction angle. Adam optimization algorithm is an adaptive learning rate optimization algorithm based on gradient stochastic objective function optimization [45]. This optimizer combines the advantages of two popular optimization methods: AdaGrad [46] for sparse gradient problems and RMSprop [47] for nonlinear and non-fixed optimization problems. Figure 5 presents a comparison of the CL algorithm's results for blind data of uniaxial compressive strength and internal friction angle across various optimizer functions.

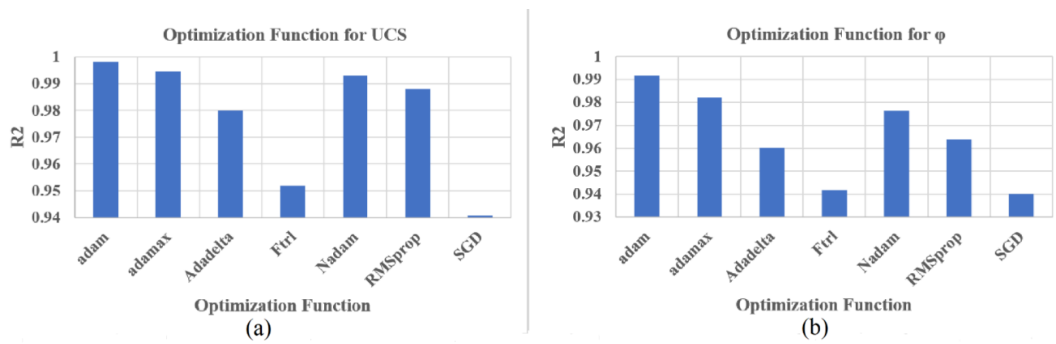

Figure 5. A comparison of the R^2 (coefficient of determination) values obtained for UCS (a) and φ angle (b) predictions with various optimizer functions using the CL algorithm for blind data.

3. Model Evaluation

The performance of the DL models for UCS and φ angle prediction are conducted by calculating widely used statistical measures as expressed in Eqs. 2, 3, 4, 5, 6, and 7. Here, mean absolute percentage error (MAPE), mean absolute error (MAE), mean squared error (MSE), root mean square error (RMSE), normalized RMS error (NMSRE), and coefficient of determination (R^2) were used to evaluate the performance of model prediction.

$$MSE = \frac{1}{n}\sum_{i=1}^{n}(Z_{mesured} - Z_{predict})^2 \tag{2}$$

$$RMSE = \sqrt{MSE} \tag{3}$$

$$NRMSE = \frac{RMSE}{MAX(Z_{mesured}) - MIN(Z_{mesured})} \tag{4}$$

$$MAE = \frac{1}{n}\sum_{i=1}^{n}|Z_{mesured} - Z_{predict}| \tag{5}$$

$$MAPE = \frac{100}{n}\sum_{i=1}^{n}\left|\frac{Z_{mesured} - Z_{predict}}{Z_{mesured}}\right| \quad (6)$$

$$R^2 = 1 - \frac{\sum_{i=1}^{n}\left(Z_{mesured} - Z_{predict}\right)^2}{\sum_{i=1}^{n}\left(Z_{mesured} - Z_{average}\right)^2} = 1 - \frac{MSE}{\sigma^2} \quad (7)$$

4. Results and Discussion

According to the core data of uniaxial compressive strength and internal friction angle in Table 2, it is necessary to generalize these parameters to all depth ranges of study. In order to generalize these samples to the entire target range (3551.072 to 3799.789 meters), at first the UCS and φ angle were calculated with the Christaras relation (equation 8) [48] and Plumb relation (equation 9) [49] using the relevant available logs. Then for the depths where the laboratory samples of UCS and φ were recorded, the relationship between the UCS and φ obtained from the logs data and laboratory results was determined. As seen in Figures 6 and 7, the derived equation for experimental and empirical UCS is a second-degree equation with an R^2 of 0.9806, while for φ angle, it is a linear equation with an R^2 of 0.9084. These two new equations, shown in Figures 6 and 7, were subsequently applied to extend the existing core test UCS and φ angle across the entire depth range under study using the related logs. Considering the high correlation coefficient obtained for uniaxial compressive strength and internal friction angle, then the calculated method has appropriate accuracy, and as a result, its generalization to all depth ranges will have appropriate accuracy. Considering the limited number of laboratory data in hydrocarbon fields, if more data are available, the results of the algorithms can be obtained with better accuracy if more data is available

$$UCS = 9.95V_p^{\,1.21} \quad (8)$$

$$\varphi = 26.5 - 37.6 \times (1 - NPHI - V_{Shale}) + 62.1 \times (1 - NPHI - V_{Shale})^2 \quad (9)$$

$$V_{shale} = \frac{GR_{log} - GR_{min}}{GR_{max} - GR_{min}} \quad (10)$$

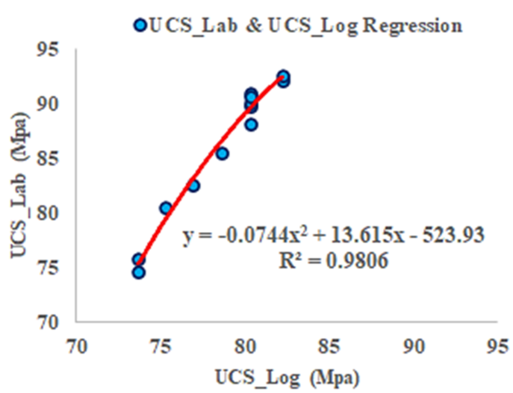

Figure 6. Relation between UCS_Log and UCS_lab.

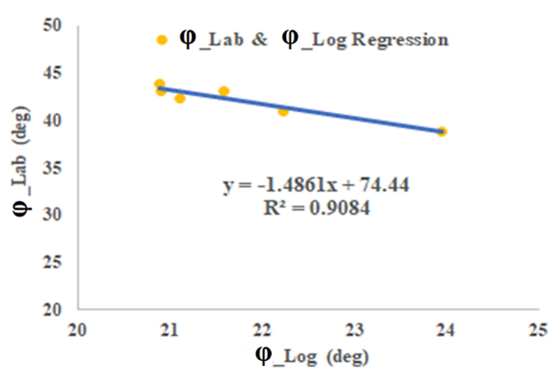

Figure 7. Relation between φ _Log and φ lab.

As stated in section 2.2.1, the UCS values were estimated with the conventional data logs of Vp, RHOB, CALIPER and NPHI and the values of φ angle were estimated with the data logs of Vp, RT, SGR and NPHI by using MLP, LSTM, CNN and CL algorithms. The log data for each case was divided into three parts, training, test, and blind, according to the procedure described in paragraph 2.2.2. Figure 8 shows the flowchart for UCS and φ estimation using four aforementioned algorithms.

Table 3 shows the parameters used in each of these MLP, LSTM, CNN and CL algorithms for UCS and Table 4 shows these parameters for φ angle prediction. Here, hyperparameters such as the optimizer function, batch size, learning rate, activation function, number of layers, kernel size, hidden layer, padding, Dropout, strides and other parameters have been tested and determined in algorithms by trial-and-error method. As an example, the selection of the best optimizer function for UCS and φ angle prediction displayed previously in Figure 5.

Tables 5 display UCS prediction errors (PE) and accuracies respectively based on the training

(80%) subsets. Here, the measured data are the data that were generalized to all depth ranges according to the available core samples. According to Table 5, for UCS training data, four algorithms have a low error, where the MSE values each of the four predicting models are equal to $MSE_{MLP} = 0.1444$, $MSE_{LSTM} = 1.4149, MSE_{CNN} = 0.1214, MSE_{CL} = 0.0651$, respectively.

Tables 6 display φ angle prediction errors and accuracies respectively based on the training (80%) subsets.

Table 7 displays the UCS prediction errors (PE) and coefficient of determination based on the test (20%) subset for four algorithms. Figures 9 provide a comparison for measured and predicted UCS using four algorithms for train and test data. According to Figure 9 and Table 5 and 7, for UCS train and test data, four algorithms MLP, LSTM, CNN and CL have a low error and high coefficient of determination, where the R^2 values for train data are equal to $R^2_{MLP} = 0.9997$, $R^2_{LSTM} = 0.9977, R^2_{CNN} = 0.9998, R^2_{CL} = 0.9999$, and R^2 values for test data are equal to $R^2_{MLP} = 0.9974$, $R^2_{LSTM} = 0.9956, R^2_{CNN} = 0.9994, R^2_{CL} = 0.9996$ respectively.

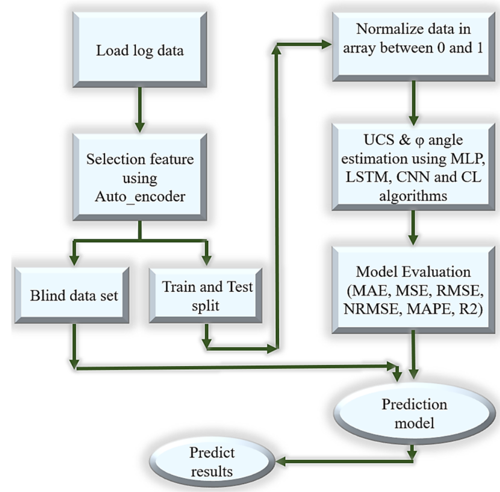

Figure 8. Workflow of UCS and φ angle prediction using MLP, LSTM, CNN, and CL algorithms and log data.

Table 3. The required parameters determined and tested in each of the algorithms for UCS prediction.

Model	Bath size	learning rate	Iteration	Optimization function	Number of hidden layers	Network architecture	Other Description
MLP	256	0.001	100	Adam	2	4-50-50-1	First hidden layer= 50 nodes Second hidden layer=50 nodes Activation function=Relu
LSTM	256	0.001	300	Adam	2	4-200-100-1	First hidden layer=200 nodes Second hidden layer=100 nodes Dropout=0.2
CNN	256	0.001	300	Adam	3	4-128-256-512-1	First layer the number of filters=128 Second layer the number of filters=256 third layer the number of filters=512 Kernel size=3, Padding= same Activation function=Relu, Strides=1
CL	512	0.01	300	Adam	4	4-128-256-64-32-1	For CNN layer: First layer the number of filters=128 Second layer the number of filters=256 Kernel size=3, Padding= same Activation function=Relu, Strides=2 For LSTM layer: First hidden layer=64 nodes Dropout=0.2 Second hidden layer=32 nodes Dropout=0.2

Table 8 displays the φ angle prediction errors and coefficient of determination based on the test (20%) subset for four algorithms. Figures 10 provide a comparison for the measured and predicted φ angle using four algorithms for train and test data. According to Figure 10 and Table 6 and 8, for φ angle train and test data, four algorithms MLP, LSTM, CNN, and CL have a low error and a high coefficient of determination, where the R^2 values for train data are equal to $R^2_{MLP} = 0.9983$, $R^2_{LSTM} = 0.9940, R^2_{CNN} = 0.9975, R^2_{CL} = 0.9987$, and R^2 values for test data are equal to $R^2_{MLP} = 0.9764$, $R^2_{LSTM} = 0.9861, R^2_{CNN} = 0.9897, R^2_{CL} = 0.9973$, respectively.

Table 4. The required parameters determined and tested in each of the algorithms for φ prediction.

Model	Bath size	learning rate	Iteration	Optimization function	Number of hidden layers	Network architecture	Other description
MLP	50	0.01	300	Adam	2	4-500-100-1	First hidden layer = 500 nodes Second hidden layer =100 nodes Activation function = Relu
LSTM	50	0.01	200	Adam	2	4-200-100-1	First hidden layer = 200 nodes Second hidden layer = 100 nodes Dropout=0.2
CNN	50	0.01	200	Adam	3	4-128-256-512-1	First layer the number of filters = 128 Second layer the number of filters = 256 third layer the number of filters=512 Kernel size=3, Padding= same Activation function=Relu, Strides=1
CL	50	0.01	300	Adam	4	4-128-256-64-32-1	For CNN layer: First layer the number of filters=128 Second layer the number of filters=256 Kernel size=3, Padding= same Activation function=Relu, Strides=2 For LSTM layer: First hidden layer=64 nodes Dropout=0.2 Second hidden layer=32 nodes Dropout=0.2

Table 5. UCS prediction errors for training data records using four algorithms.

PE	MLP	LSTM	CNN	CL
MAE	0.1841	0.8085	0.2705	0.1352
MAPE	1.5523	5.5421	0.5669	0.7862
MSE	0.1444	1.4149	0.1214	0.0651
RMSE	0.3801	1.1895	0.3485	0.2552
NRMSE	0.0035	0.0110	0.0032	0.0023
R^2	0.9997	0.9977	0.9998	0.9999

Table 6. Internal friction angle prediction errors for training data using four algorithms.

PE	MLP	LSTM	CNN	CL
MAE	0.3267	0.5384	0.3388	0.0491
MAPE	1.2062	2.4101	1.5149	0.4536
MSE	0.1538	0.6119	0.2319	0.0037
RMSE	0.3921	0.7822	0.4815	0.0610
NRMSE	0.0092	0.0183	0.0113	0.0081
R^2	0.9983	0.9940	0.9975	0.9987

Table 7. UCS prediction errors and coefficient of determination for test data.

PE	MLP	LSTM	CNN	CL
MAE	0.5817	1.2700	0.4140	0.2862
MAPE	0.8287	2.7277	0.7331	0.5829
MSE	1.8988	2.2533	0.4522	0.3065
RMSE	1.3779	1.5011	0.6724	0.5536
NRMSE	0.0151	0.0201	0.0073	0.0060
R^2	0.9974	0.9956	0.9994	0.9996

Table 8. Internal friction angle prediction errors and coefficient of determination for test data.

PE	MLP	LSTM	CNN	CL
MAE	1.2560	0.5543	0.4873	0.1064
MAPE	4.5164	1.9126	2.1156	2.1869
MSE	2.4007	0.8780	0.8328	0.0219
RMSE	1.5494	0.9370	0.91260	0.1480
NRMSE	0.0363	0.0252	0.0245	0.0127
R^2	0.9764	0.9861	0.9897	0.9973

At this stage, the validation of the algorithms has been applied to previously unseen (blind) data. Table 9 depicts the predicted UCS errors and coefficient of determination based on the blind subsets of data, selected from the 400 data records. To estimate uniaxial compressive strength, error values for blind data are equal to $MSE_{MLP} = 47.2230$, $MSE_{LSTM} = 8.1027, MSE_{CNN} = 1.9375, MSE_{CL} = 1.0105$, and determination coefficient values are equal to $R^2_{MLP} = 0.9186$, $R^2_{LSTM} = 0.9860, R^2_{CNN} = 0.9966, R^2_{CL} = 0.9983$.

Figure 11 shows a comparison of the predicted UCS using four algorithms with the measured UCS values for blind dataset.

Table 9. UCS prediction errors for blind data records using four algorithms.

PE	MLP	LSTM	CNN	CL
MAE	5.8694	1.8388	1.2671	0.8974
MAPE	15.4218	13.9033	2.9906	1.9769
MSE	47.2230	8.1027	1.9375	1.0105
RMSE	6.8719	2.8465	1.3919	1.0052
NRMSE	0.0640	0.0265	0.0129	0.0093
R^2	0.9186	0.9860	0.9966	0.9983

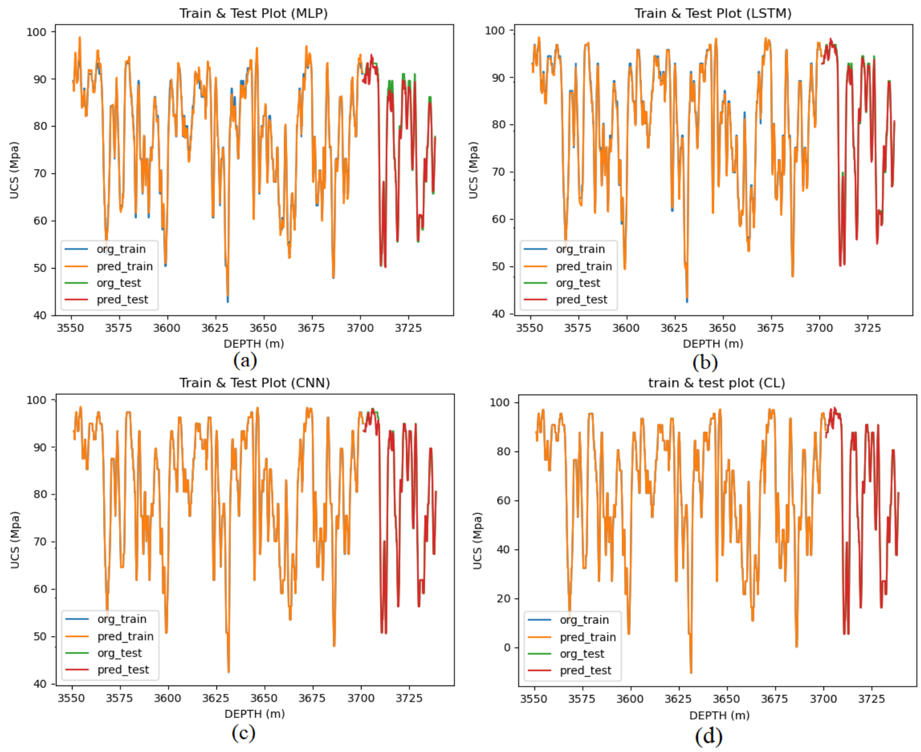

Figure 9. Comparison of the predicted UCS using four algorithms with the measured UCS for train and test data. (a), MLP algorithm. (b), LSTM algorithm. (c), CNN algorithm, (c), CL algorithm. Blue log (measured UCS for training (original data)), orange log (predicted UCS for training data), green log (measured UCS for test data (original data)), red log (predicted UCS for test data).

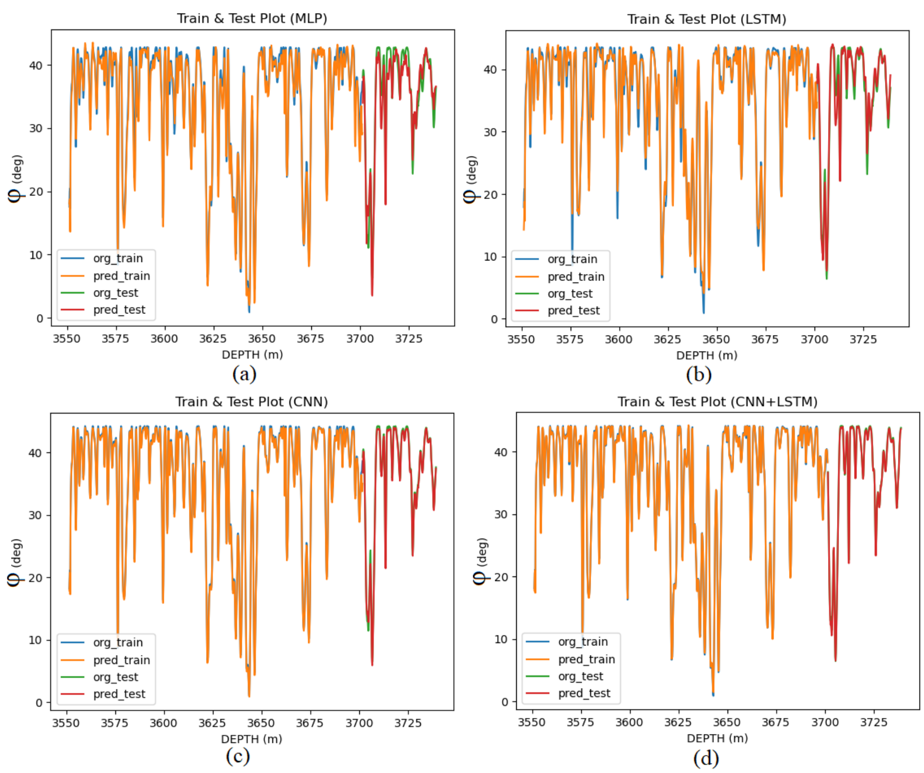

Figure 10. Comparison of the predicted φ angle using four algorithms with the measured φ angle for train and test data (a), prediction of φ angle using MLP algorithm (b) prediction of φ angle using LSTM. (c), prediction of φ angle using CNN. (c), prediction of φ angle using CL. Blue log (measured φ angle for training (original data)), orange log (predicted φ angle for training data), green log (measured φ angle for test data (original data)), red log (predicted φ angle for test data).

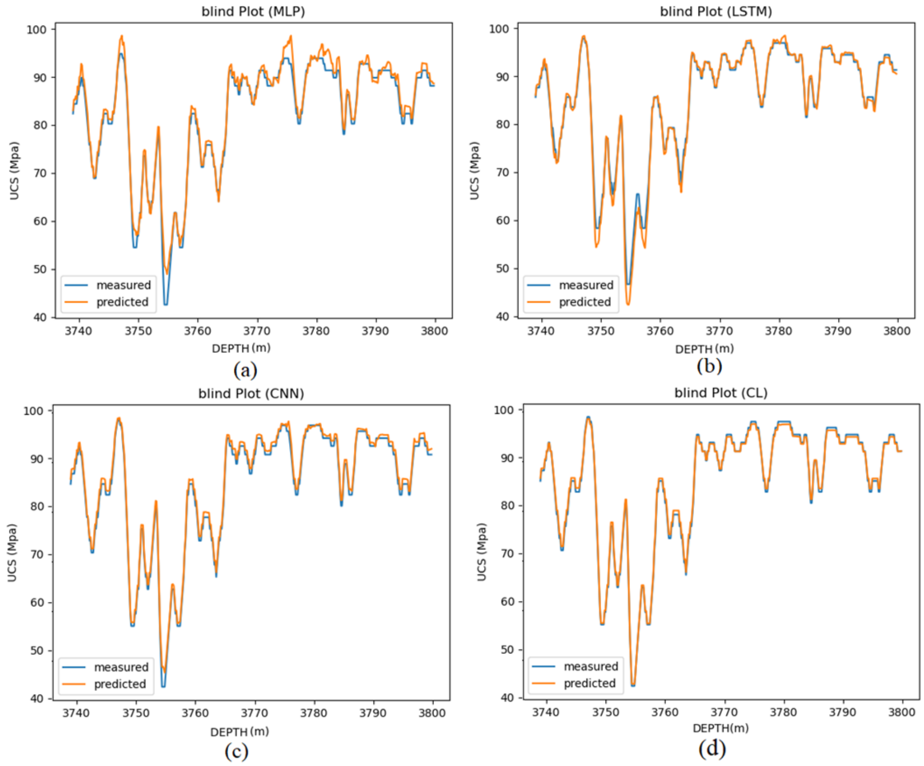

Figure 11. Comparison of the predicted UCS values using four (MLP, LSTM, CNN and CL) deep learning algorithms with the measured UCS values of the blind dataset. (a), UCS prediction using MLP. (b), UCS prediction using LSTM. (c), UCS prediction using CNN, (c), UCS prediction using CL.

Figure 12 shows the coefficient of determination of the blind data of the UCS measured and the UCS predicted by four algorithms. According to the values of Table 9 and considering the prediction errors and the coefficient of determination, it can be concluded that the most robust and best method of UCS prediction is the CL algorithm and the weakest performance for this case related to the MLP algorithm.

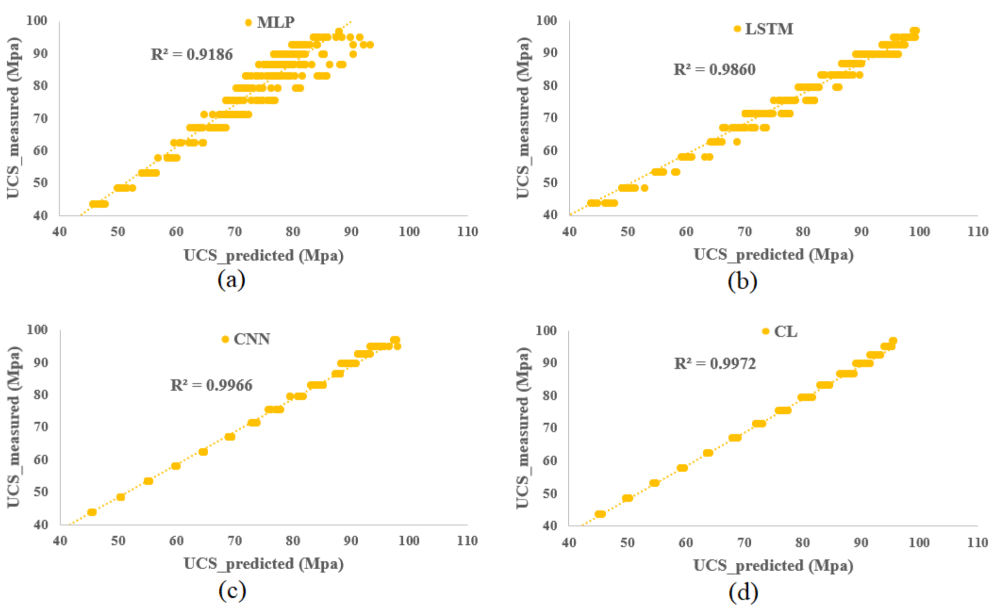

Figure 12. Display of coefficient of determination of blind data for measured and predicted UCS using four algorithms. (a) R^2 using MLP algorithm (b) R^2 using LSTM algorithm (c)R^2 using CNN algorithm (c) R^2 using CL algorithm

Table 10 depicts the predicted φ angle errors and coefficient of determination based on the blind sub-sets of data. To estimate φ angle, error values for blind data are equal to $MSE_{MLP} = 5.5839$, $MSE_{LSTM} = 3.0233$, $MSE_{CNN} = 1.9882$, $MSE_{CL} = 0.0230$, and determination coefficient values are equal to $R^2_{MLP} = 0.9117$, $R^2_{LSTM} = 0.9522$, $R^2_{CNN} = 0.9686$, $R^2_{CL} = 0.9917$.

Figure 13 shows a comparison of the predicted φ angle using four algorithms with the measured φ angle for blind data. Figure 14 shows the coefficient of determination of the blind data of the measured and the predicted φ angle for four algorithms. According to the values of Table 10, and considering the prediction errors and the coefficient of determination, it can be concluded that the most robust and best method of φ angle prediction is the CL algorithm and the weakest performance for this case related to the MLP algorithm.

Table 10. Internal friction angle prediction errors for blind data records using four algorithms.

PE	MLP	LSTM	CNN	CL
MAE	1.5556	1.2357	0.8901	0.1333
MAPE	4.5404	4.2019	3.3746	1.3088
MSE	5.5839	3.0223	1.9882	0.0230
RMSE	2.3630	1.7385	1.4100	0.1517
NRMSE	0.0636	0.0468	0.0379	0.0201
R^2	0.9117	0.9522	0.9686	0.9917

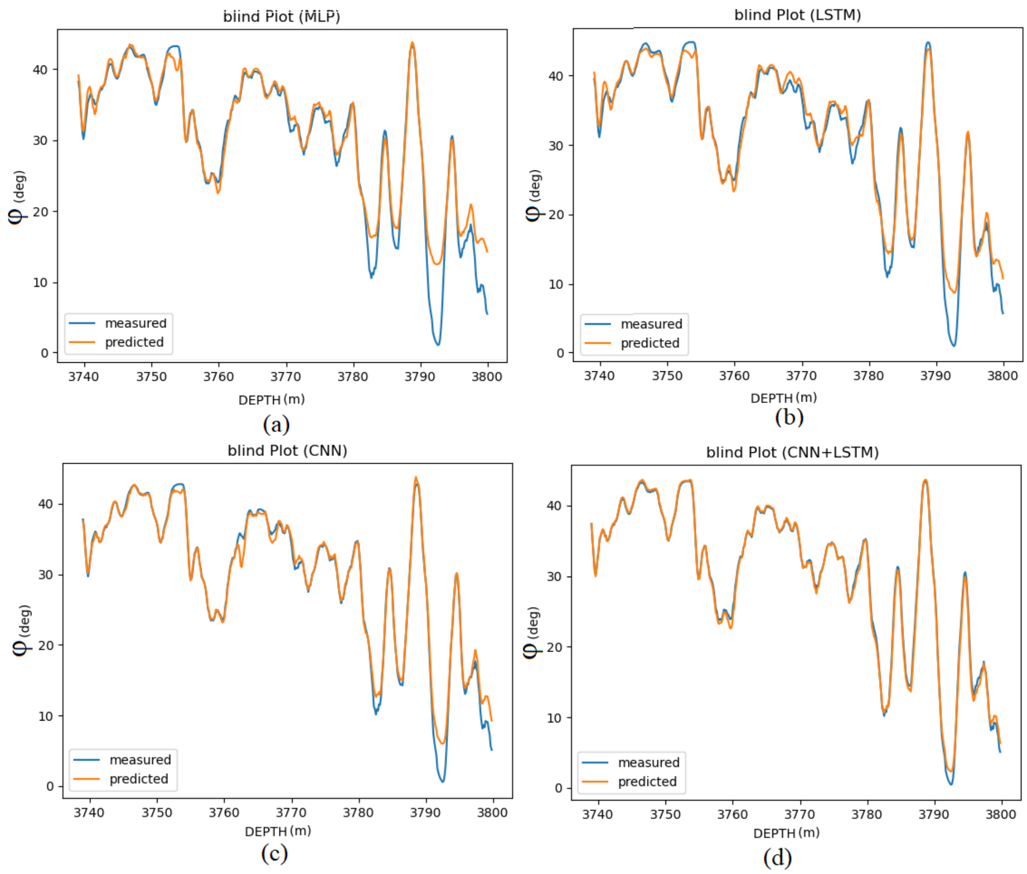

Figure 13. Comparison of the predicted φ angle values using four (MLP, LSTM, CNN, and CL) deep learning algorithms with the measured φ angle values of the blind dataset (a) φ prediction using MLP (b), φ prediction using LSTM (c) φ prediction using CNN (d), φ prediction using CL.

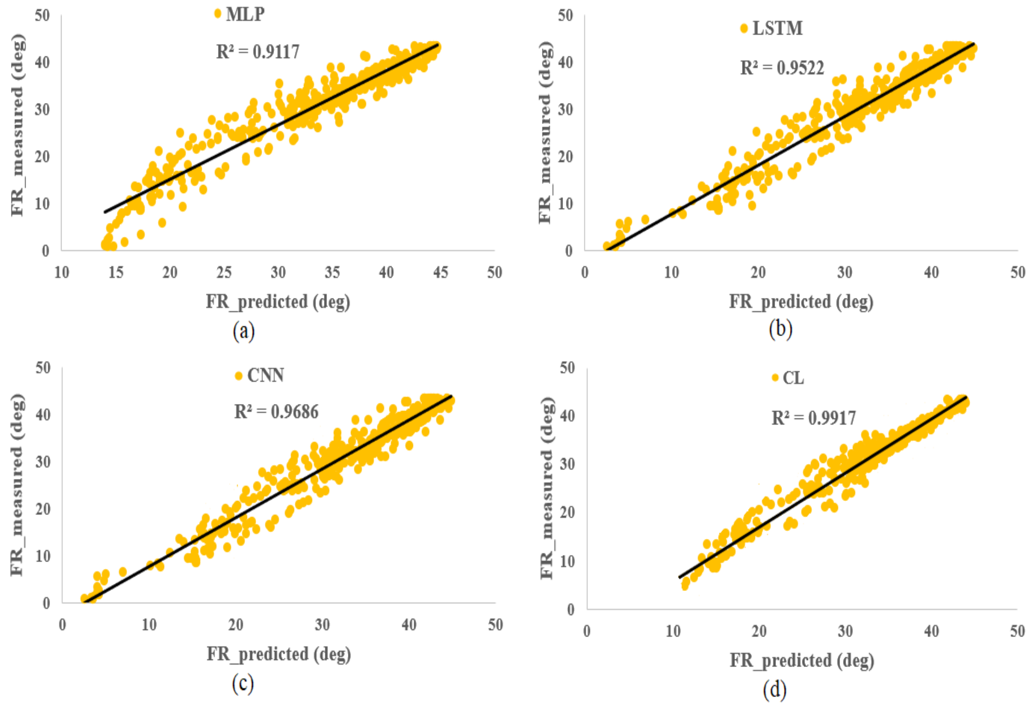

Figure 14. Display of coefficient of determination of blind data for φ measured and φ predicted using four algorithms (a) R^2 using MLP algorithm (b) R^2 using LSTM algorithm (c) R^2 using CNN algorithm (c) R^2 using CL algorithm.

To further assess the performance of the four deep learning models, a sub-set of the estimated UCS and φ angle values from the blind dataset, along with the actual values, is presented in Figure 15. As illustrated in Figure 15, while all the deep learning algorithms perform sufficiently well, the CL model yields more accurate estimates for both UCS and φ angle compared to the other models.

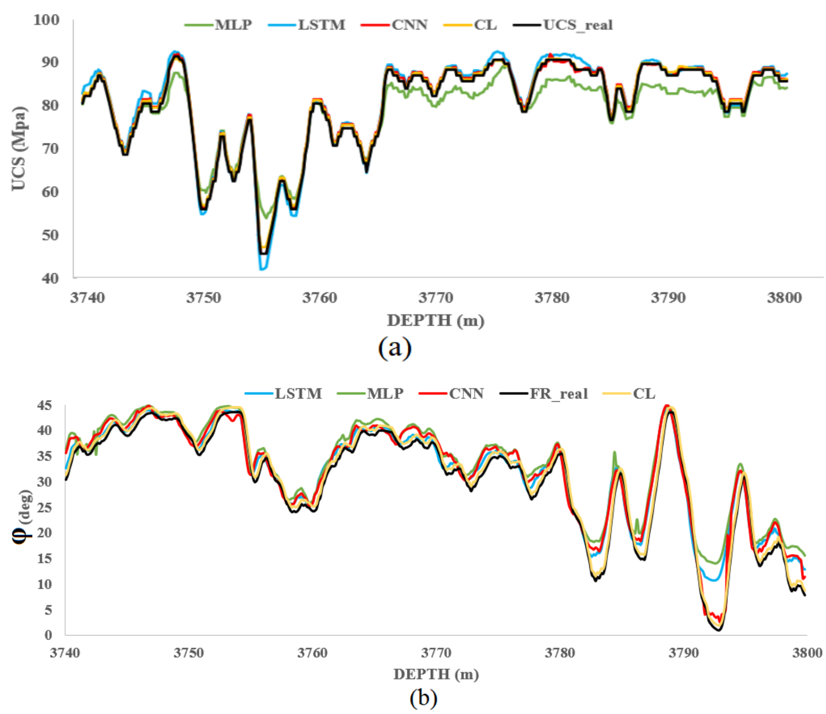

Figure 15. Comparing the estimated values of UCS and φ angle with four algorithms MLP, LSTM, CNN, and CL and real data (a) Uniaxial compressive strength (b) internal friction angle

In addition, the test plot of 10 selected absolute errors (Figure 16) and the overall RMS error plot (Figure 17) for UCS and φ angle predictions using the four deep learning models—MLP, LSTM, CNN, and CL—and their comparison with actual data show that the CL algorithm achieves the lowest absolute and RMS error among the models in prediction.

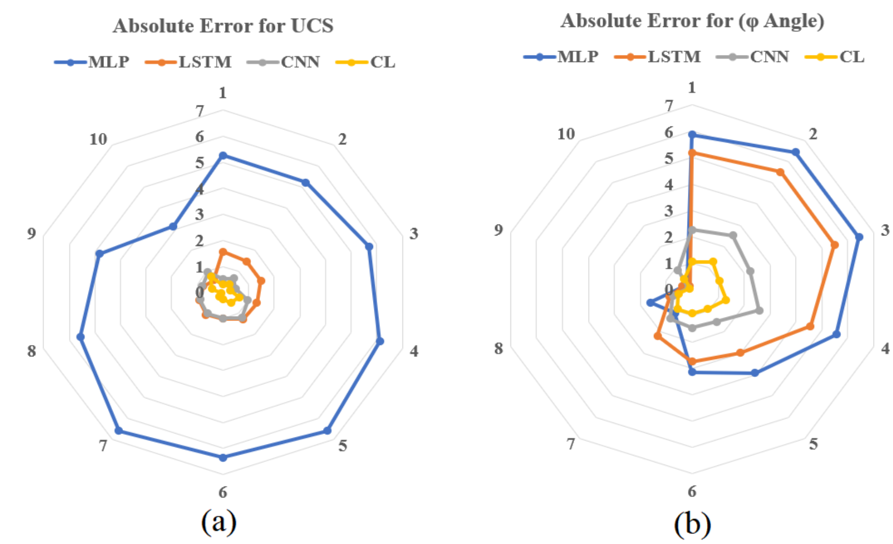

Figure 16. The absolute error diagram of 10 selected samples of uniaxial compressive strength and internal friction angle predicted by four algorithms MLP, LSTM, CNN, and CL and real data of blind dataset (a) Uniaxial compressive strength (b) internal friction angle.

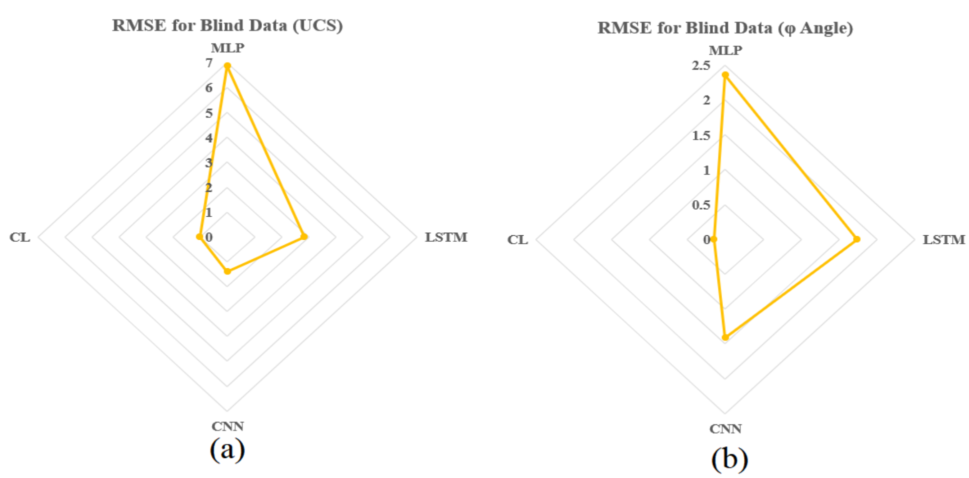

Figure 17. The overall RMSE diagram of uniaxial compressive strength and internal friction angle estimation using four algorithms MLP, LSTM, CNN and CL for blind data (a) Uniaxial compressive strength (b) internal friction angle.

Finally, Table 11 presents the results of various methods previously developed by researchers for determining the uniaxial compressive strength and internal friction angle of rock and soil, along with the results of three (Cheristaras [48] (equation 8), Yaser and Erdogan [56], (Equation 11) and Tercan [57], (Equation 12)) empirical methods and four intelligent models applied in this study for comparison. As shown, the four intelligent methods used in this study demonstrate very low error rates and high correlation coefficients in predicting these geomechanical parameters when compared to actual data. This indicates the strong accuracy of the deep learning methods introduced here, especially with the application of the CL hybrid approach.

$$UCS = 21.677V_p + 0.0648 \quad (11)$$

$$UCS = 7.1912V_p + 26.258 \quad (12)$$

Table 11. Comparing the results of several previous studies with the results obtained from current study.

Reference	ML /empirical methods	Input variables	Parameter	MSE	MAE	RMSE	R^2
Gokceoglu and Zorlu [10]	FIS*, MR	Apparent Porosity, Vp, Schmidt Hardness, Tensile Strength, Point Load Index, Block Punch Index	UCS			13.6	0.8124
Dadhich et al [29]	ANN*, MLR, RFR	Point load strength, porosity, Schmidt rebound hardness, block punch index, and specific gravity.	UCS		9.79		0.92
Xu et al [50]	SSA-XGBoost*, XGBoost, SVM, RF, …	Porosity, Schmidt rebound number, Vp and point load strength	UCS		14.79	19.85	0.84
Kochukrishnan et al [51]	LR, SWR*	Ultrasonic Pulse Velocity (UPV), Schmidt Hammer Rebound Number (N), Brazilian Tensile Strength (BTS), and Point Load Index (PLI)	UCS		2.71	3.6	0.99
Zhao et al. [52]	XGBoost-ABC*, RF, ANN	Rock density, P-wave velocity, and point load strength index	UCS		3.76	4.78	0.93
Daniel et al. [53]	EL*, AdaBoost, GBDT, XGBoost, LightGBM, RF, ET*	Schmidt hammer rebound number, P-wave velocity, and point load index data,	UCS		4.0656	5.2024	0.9854
Niu et al. [54]	KNN, KNIM*, KNAF	Schmidt hammer rebound number, bulk density, bulk tensile strength, dry density test, (Vp), and point load index test	UCS	19.245		4.387	0.986
Kalabarige et al. [55]	VR*, DT, SVM, LR, KNN, LGBM, XGB, RF, ETR, BagXGB, BagETR	cement (C), LP, FA, GGBS, SFs, RHA, MP, BP, CA, fine aggregate (Fa), RCA, W, SP, and VMA	UCS	21.74	3.42	4.66	0.9243
This research (using Cheristaras [48] Eq.)	$UCS = 9.95V_p^{\ 1.21}$	Vp	UCS	248.0327	12.1019	15.7490	0.5201
This research (using Yaser and Erdogan [56] Eq.)	$\text{UCS} = 21.677V_p + 0.0648$	Vp	UCS	2144.471	44.4911	46.3084	0.0314
This research (using Tercan [57] Eq.)	$\text{UCS} = 7.1912V_p + 26.258$	Vp	UCS	398.2935	17.3208	19.9572	0.2294
Khanlari et al [56]	MVR, ANN*	Percentages of passing the No. 200 (≠ 200), 40 (≠40) and 4 (≠4) sieves, plasticity index (PI), and density (ρ)	φ		1.92	2.26	0.792
Iyeke et al. [57]	ANN	Grain size distribution, plastic limit, liquid limit, specific gravity, compaction, shear box tests and triaxial compression tests	φ		4.34	4.77	0.805
Mohammadi et al. [58]	MLR, MLP*	Atterberg limits, density, percentages of gravel, sand, silt, clay and passing the sieves No. 200	φ		6.137	9.285	0.814
Pham et al. [33]	DNN, PSO_DNN*	soil state, standard penetration test value, unit weight of soil, void ratio, thickness of soil layer, top elevation of soil layer, and bottom elevation of soil layer	φ		1.425	1.936	0.935
Shahani et al. [36]	LR, RR, DT, SVM*	P-wave velocity in (m/s), density in (gm/cc), UCS in (MPa), and tensile strength in (MPa)	φ	1.7958	1.0021	1.3401	0.912
This research (for blind data)	MLP, LSTM, CNN, CL*	Vp, RHOB, CALIPER, and NPHI logs and core data	UCS	1.0105	0.8974	1.0052	0.9983
This research (for blind data)	MLP, LSTM. CNN, CL*	Vp, LL7 (RT), SGR, and NPHI logs and core data	φ	0.0230	0.1333	0.0201	0.9917

Statistical evaluation parameters: MSE, MAE, RMSE, R^2.

* The algorithm with the best result

It should be noted that previous studies mentioned in Table 11 have mainly focused on using laboratory tests conducted on rock/ soil or concrete samples, which are either limited or rarely available for oil reservoir studies. However, in this study, as an alternative to relying on only limited core sample test results, conventional well log data was used to predict the specified rock parameters. The deep learning algorithm is one of the new and high-accuracy methods for predicting UCS and φ angle. In this study, four algorithms (MLP, LSTM, CNN and CL) are used to predict UCS and φ angle values. The results show the high accuracy of LSTM, CNN and CL algorithms for UCS and φ angle prediction. Therefore, the accuracy and robustness of the prediction results of these algorithms have more advantages than MLP algorithm and traditional empirical models.

5. Conclusions

Uniaxial compressive strength and friction angle of rock are of the most practical geomechanical and engineering parameters, which is an urgent requirement for engineers in most designs and modeling tasks. In this study, some models are established for predicting UCS and φ angle values based on three MLP, LSTM, CNN and CL algorithms. To achieve the goals, first, the auto-encoder algorithm was used to select the effective features. Based on the acquired results, the best effective features logs for UCS predication were the values of density, neutron, sonic and caliper logs while for φ angle prediction the neutron, sonic, resistivity and gamma ray logs were selected as the best feature logs. In the next step, the model was defined and trained using four: MLP, LSTM, CNN and CL algorithms. To estimate the uniaxial compressive strength, the structure of the MLP model including two hidden layers and each layer including 50 nodes, the LSTM model including two layers where the first layer has 200 nodes and the second layer has 100 nodes and the dropout is 0.2, and for CNN model consists of three layers, 128 filters of the first layer, 256 filters of the second layer and 512 filters of the third layer were selected and for CL model consists of four layers, two CNN and two LSTM layers were selected. To estimate the internal friction angle, the number of layers was chosen similar to uniaxial compressive strength, but in the MLP model, the first layer has 500 nodes and the second layer has 100 nodes. Although other parameters such as batch size, learning rate and iteration were chosen differently for these two parameters. To ensure the results of the algorithms, the evaluation of the models was done with some errors parameters and R^2 value. In the next step, the four models were also applied on the blind dataset, their error values obtained as; $MSE_{MLP} = 47.2230$, $MSE_{LSTM} = 8.1027, MSE_{CNN} = 1.9375, MSE_{CL} = 1.0105$ and their R^2 values as; $R^2_{MLP} = 0.9186$, $R^2_{LSTM} = 0.9860$, $R^2_{CNN} = 0.9966, R^2_{CL} = 0.9983$ for the UCS prediction. For the φ angle of blind data, $MSE_{MLP} = 5.5839$, $MSE_{LSTM} = 3.0233, MSE_{CNN} = 1.9882, MSE_{CL} = 0.0230$ and R^2 values of; $R^2_{MLP} = 0.9117$, $R^2_{LSTM} = 0.9522, R^2_{CNN} = 0.9686, R^2_{CL} = 0.9917$ were obtained. Moreover, the UCS and φ angle are predicted by the proposed and traditional empirical models. It has been demonstrated that the introduced and deigned LSTM, CNN and CL deep learning models, outperforms the MLP and traditional empirical models in their prediction accuracy and robustness. While MLP method achieved relatively satisfactory results in UCS and φ angle prediction, but compared to the LSTM, CNN and CL algorithms, it shows less accuracy and more error. In short, it can be stated that the designed CNN, LSTM and CL deep learning models have much better performance than the MLP model for UCS and φ angle continuous prediction using the relevant well log data. Despite the limited number of core samples used in this study, various evaluation methods demonstrated the effectiveness of the proposed DL models, especially the accuracy of the CL hybrid algorithm for predicting UCS and φ angle values from conventional well log data. Certainly, if data from additional wells in diverse geological locations and more core and log samples were available, these DL models could yield results that generalize more effectively to the broader geological conditions of the oil field. It is therefore recommended to apply the proposed and other deep learning algorithms with an expanded dataset of uniaxial compressive strength and internal friction angle, along with integrating geological information into the data, to achieve even higher prediction accuracy.

Abbreviations

ACE	Alternative condition expectation
AFT	Alibaba and the Forty Thieves
AI	Artificial intelligence
ANFIS	Adaptive neuro-fuzzy inference
ANN	Artificial neural network
APSO	Aarticle swarm optimization algorithm with adaptive learning strategy
ASR	Automatic speech recognition
BA	Bayesian algorithm
BagXGB	XGB-based bagging
BPANN	Backpropagation artificial neural network
BTS	Brazilian tensile strength
CFBNN	Conventional feedforward backpropagation neural network Cumulative distribution functions
CHAL	Caliper log
CFM	Committee fuzzy machine
CMIS	Committee machine with intelligent systems
CL	CNN+LSTM
CNL	Compensate neutron log
CNN	Convolutional neural network
DBN	Deep Belief Network
DL	Deep learning
DNN	Deep neural network
DSI	Dipole Shear Sonic Imaging

DT	Acoustic (sonic) log
ELM	Extreme learning machine
ENN	Elman neural network
FFANN	Feedforward artificial neural network
FL	Fuzzy logic
FR	Friction angle
φ	Friction angle
GA	Genetic algorithm
GBR	Gradient boosting regression
GBRT	gradient boosted tree regressor
GEP	Gene expression programming
GR	Gamma ray log
GRA	Grey relational analysis LSTM Long short-term memory networks
GRG	Generalized reduced gradient
GRNN	General regression neural network
HTS	hydraulic tensile strength
IMRFO	Improved Manta-Ray Foraging Optimization
KNN	K-Nearest Neighbour
LightGBM	light gradient boosting machine
LSSVM	Least-squares support-vector machines
LSTM	Long short-term memory networks
MAE	Mean absolute error
MAPE	Mean absolute percentage error
MF	Memetic firefly
MGGP	multi-gene genetic programming
ML	Machine learning technique
MLEM	Multi extreme learning machine
MELM	Multi-layer Extreme Learning Machine
MLP	Multi-layer perceptron
MPMR	minimax probability machine regression
MSE	Mean square error
NARX	Nonlinear autoregressive network with exogenous inputs
NEUT	Neutron porosity
NF	neuro-fuzzy
NRMSE	Normalized Root Mean Squared Error
OFIS	Optimized fuzzy inference
ONN	Optimized neural network
OSVR	Optimized support vector regression
PERM	Permeability log
PSO	Particle swarm optimization
R2	Coefficient of determination
RHOB	Density log
RMSE	Root mean square error
RNN	Recurrent neutral network
RS	Shallow lateral resistivity log
RT	Formation true resistivity
RVM	relevance vector machine
SFIS	Surgeon's fuzzy inference
SML	Single machine learning
SSA-XGBoost	Sparrow Search Algorithm- Extreme Gradient Boosting
SVM	Support vector machine
SVR	Support vector regression
UCS	uniaxial compressive strength
Vs	Shear wave velocity
Vp	Compressional wave velocity
XGB	extreme gradient boost

References

[1] Cargill, J. S., & Shakoor, A. (1990, December). Evaluation of empirical methods for measuring the uniaxial compressive strength of rock. In *International Journal of Rock Mechanics and Mining Sciences & Geomechanics Abstracts* (Vol. 27, No. 6, pp. 495-503). Pergamon.

[2] Tuğrul, A., & Zarif, I. H. (1999). Correlation of mineralogical and textural characteristics with engineering properties of selected granitic rocks from Turkey. *Engineering geology*, *51*(4), 303-317.

[3] Karakus, M., & Tutmez, B. (2006). Fuzzy and multiple regression modelling for evaluation of intact rock strength based on point load, Schmidt hammer and sonic velocity. *Rock mechanics and rock engineering*, *39*, 45-57.

[4] Yagiz, S. (2011). P-wave velocity test for assessment of geotechnical properties of some rock materials. *Bulletin of Materials Science*, *34*, 947-953.

[5] Singh, R., Vishal, V., Singh, T. N., & Ranjith, P. G. (2013). A comparative study of generalized regression neural network approach and adaptive neuro-fuzzy inference systems for prediction of unconfined compressive strength of rocks. *Neural Computing and Applications*, *23*, 499-506.

[6] Aladejare, A. E. (2020). Evaluation of empirical estimation of uniaxial compressive strength of rock using measurements from index and physical tests. *Journal of Rock Mechanics and Geotechnical Engineering*, *12*(2), 256-268.

[7] Hazbeh, O., Rajabi, M., Tabasi, S., Lajmorak, S., Ghorbani, H., Radwan, A. E., & Molaei, O. (2024). Determination and investigation of shear wave velocity based on one deep/machine learning technique. *Alexandria Engineering Journal*, *92*, 358-369.

[8] Mollaei, F., Moradzadeh, A., & Mohebian, R. (2024). Estimation brittleness index in carbonate environments using log and lithology data and deep learning techniques. *Italian journal of engineering geology and environment*, (1), 49-66.

[9] Mollaei, F., Moradzadeh, A., & Mohebian, R. (2024). Novel approaches in geomechanical parameter estimation using machine learning methods and conventional well logs. *Geosystem Engineering*, *27*(5), 252-277.

[10] Gokceoglu, C., & Zorlu, K. (2004). A fuzzy model to predict the uniaxial compressive strength and the modulus of elasticity of a problematic rock. *Engineering Applications of Artificial Intelligence*, *17*(1), 61-72.

[11] Yilmaz, I., & Yuksek, A. G. (2008). An example of artificial neural network (ANN) application for indirect estimation of rock parameters. *Rock Mechanics and Rock Engineering*, *41*(5), 781-795.

[12] Tiryaki, B. (2008). Predicting intact rock strength for mechanical excavation using multivariate statistics, artificial neural networks, and regression trees. *Engineering Geology*, *99*(1-2), 51-60.

[13] Sarkar, K., Tiwary, A., & Singh, T. N. (2010). Estimation of strength parameters of rock using artificial neural networks. *Bulletin of engineering geology and the environment*, *69*, 599-606.

[14] Dehghan, S., Sattari, G. H., Chelgani, S. C., & Aliabadi, M. A. (2010). Prediction of uniaxial compressive

strength and modulus of elasticity for Travertine samples using regression and artificial neural networks. *Mining Science and Technology (China)*, *20*(1), 41-46.

[15] Manouchehrian, A., Sharifzadeh, M., & Moghadam, R. H. (2012). Application of artificial neural networks and multivariate statistics to estimate UCS using textural characteristics. *International Journal of Mining Science and Technology*, *22*(2), 229-236.

[16] Rabbani, E., Sharif, F., Koolivand Salooki, M., & Moradzadeh, A. (2012). Application of neural network technique for prediction of uniaxial compressive strength using reservoir formation properties. *International journal of rock mechanics and mining sciences*, *56*, 100-111.

[17] Singh, T. N., & Verma, A. K. (2012). Comparative analysis of intelligent algorithms to correlate strength and petrographic properties of some schistose rocks. *Engineering with Computers*, *28*, 1-12.

[18] Yesiloglu-Gultekin, N., Gokceoglu, C., & Sezer, E. A. (2013). Prediction of uniaxial compressive strength of granitic rocks by various nonlinear tools and comparison of their performances. *International Journal of Rock Mechanics and Mining Sciences*, *62*, 113-122.

[19] Majdi, A., & Rezaei, M. (2013). Prediction of unconfined compressive strength of rock surrounding a roadway using artificial neural network. *Neural Computing and Applications*, *23*, 381-389.

[20] Mishra, D. A., & Basu, A. (2013). Estimation of uniaxial compressive strength of rock materials by index tests using regression analysis and fuzzy inference system. *Engineering Geology*, *160*, 54-68.

[21] Rezaei, M., Majdi, A., & Monjezi, M. (2014). An intelligent approach to predict unconfined compressive strength of rock surrounding access tunnels in longwall coal mining. *Neural Computing and Applications*, *24*, 233-241.

[22] Mohamad, E. T., Jahed Armaghani, D., Momeni, E., & Alavi Nezhad Khalil Abad, S. V. (2015). Prediction of the unconfined compressive strength of soft rocks: a PSO-based ANN approach. *Bulletin of Engineering Geology and the Environment*, *74*, 745-757.

[23] Armaghani, D. J., Safari, V., Fahimifar, A., Mohd Amin, M. F., Monjezi, M., & Mohammadi, M. A. (2018). Uniaxial compressive strength prediction through a new technique based on gene expression programming. *Neural Computing and Applications*, *30*, 3523-3532.

[24] Saedi, B., Mohammadi, S. D., & Shahbazi, H. (2018). Prediction of uniaxial compressive strength and elastic modulus of migmatites using various modeling techniques. *Arabian Journal of Geosciences*, *11*, 1-14.

[25] Rezaei, M., & Asadizadeh, M. (2020). Predicting unconfined compressive strength of intact rock using new hybrid intelligent models. *Journal of Mining and Environment*, *11*(1), 231-246.

[26] Wang, M., & Wan, W. (2019). A new empirical formula for evaluating uniaxial compressive strength using the Schmidt hammer test. *International Journal of Rock Mechanics and Mining Sciences*, *123*, 104094.

[27] Fattahi, H. (2020). A new method for forecasting uniaxial compressive strength of weak rocks. *Journal of Mining and Environment*, *11*(2), 505-515.

[28] Hassan, M. Y., & Arman, H. (2022). Several machine learning techniques comparison for the prediction of the uniaxial compressive strength of carbonate rocks. *Scientific reports*, *12*(1), 20969.

[29] Dadhich, S., Sharma, J. K., & Madhira, M. (2022). Prediction of uniaxial compressive strength of rock using machine learning. *Journal of The Institution of Engineers (India): Series A*, *103*(4), 1209-1224.

[30] Afolagboye, L.O., Ajayi, D.E. and Afolabi, I.O. (2023). Machine learning models for predicting unconfined compressive strength: A case study for Precambrian basement complex rocks from Ado-Ekiti, Southwestern Nigeria, Scientific African.

[30] Afolagboye, L. O., Ajayi, D. E., & Afolabi, I. O. (2023). Machine learning models for predicting unconfined compressive strength: A case study for Precambrian basement complex rocks from Ado-Ekiti, Southwestern Nigeria. *Scientific African*, *20*, e01715.

[31] Ibrahim, A. F., Hiba, M., Elkatatny, S., & Ali, A. (2024). Estimation of tensile and uniaxial compressive strength of carbonate rocks from well-logging data: artificial intelligence approach. *Journal of Petroleum Exploration and Production Technology*, *14*(1), 317-329.

[32] Alloush, R.M., Elkatatny, S.M., Mahmoud, M.A., Moussa, T.M., Ali, A.Z. and Abdulraheem, A. (2017). Estimation of Geomechanical Failure parameter from well logs using artificial intelligence techniques, SPE.

[32] Alloush, R. M., Elkatatny, S. M., Mahmoud, M. A., Moussa, T. M., Ali, A. Z., & Abdulraheem, A. (2017). Estimation of geomechanical failure parameters from well logs using artificial intelligence techniques. In *SPE Kuwait Oil and Gas Show and Conference* (p. D031S010R002). SPE.

[33] Pham, T. A., Tran, V. Q., & Vu, H. L. (2021). Evolution of deep neural network architecture using particle swarm optimization to improve the performance in determining the friction angle of soil. *Mathematical Problems in Engineering*, *2021*(1), 5570945.

[34] Hiba, M., Ibrahim, A. F., Elkatatny, S., & Ali, A. (2022). Prediction of cohesion and friction angle from well-logging data using decision tree and random forest. *Arabian Journal of Geosciences*, *15*(1), 26.

[35] Faraj, A. K., Abdul Hussein, H. A. H., & Abed Al-Hasnawi, A. N. (2022). Estimation of Internal Friction Angle for The Third Section in Zubair Oil Field: A Comparison Study. *Iraqi Journal of Oil and Gas Research (IJOGR)*, *2*(2), 102-111.

[36] Shahani, N. M., Ullah, B., Shah, K. S., Hassan, F. U., Ali, R., Elkotb, M. A., ... & Tag-Eldin, E. M. (2022). Predicting angle of internal friction and cohesion of rocks based on machine learning algorithms. *Mathematics*, *10*(20), 3875.

[37] Nguyen, T., Shiau, J., & Ly, D. K. (2024). Enhanced earth pressure determination with negative wall-soil

friction using soft computing. *Computers and Geotechnics*, *167*, 106086.

[38] Alavi, A.H., Gandomi, A.H., Mollahassani, A., Akbar Heshmati, A., & Rashed, A. (2010). Modeling of maximum dry density and optimum moisture content of stabilized soil using artificial neural networks. *Journal of Plant Nutrition and Soil Science*, *173*(3), 368-379.

[39] Phyo, P. P., & Byun, Y. C. (2021). Hybrid ensemble deep learning-based approach for time series energy prediction. *Symmetry*, *13*(10), 1942.

[40] Hochreiter, S. & Schmidhuber, J. (1997). Long short-term memory. *Neural Comput. 9* (8), 1735–1780.

[41] Greff, K., Srivastava, R. K., Koutník, J., Steunebrink, B. R., & Schmidhuber, J. (2016). LSTM: A search space odyssey. *IEEE transactions on neural networks and learning systems*, *28*(10), 2222-2232.

[42] Guo, Y., Liu, Y., Oerlemans, A., Lao, S., Wu, S., & Lew, M. S. (2016). Deep learning for visual understanding: A review. *Neurocomputing*, *187*, 27-48.

[43] Lecun, Y., Bottou, L., Bengio, L. & Haffner, P. (1998). Gradient -based learning applied to document recognition", *Proceedings of the IEEE, 86,(11),* 2278 –2324.

[44] Anemangely, M., Ramezanzadeh, A., Amiri, H., & Hoseinpour, S. A. (2019). Machine learning technique for the prediction of shear wave velocity using petrophysical logs. *Journal of Petroleum Science and Engineering*, *174*, 306-327.

[45] Kingm, D.P., & Ba, J. (2014). Adam: A Method for Stochastic Optimization. *https://arxiv. org*/abs/1412.6980.

[46] Duchi, J., Hazan, E., & Singer, Y. (2011). Adaptive subgradient methods for online learning and stochastic optimization. *Journal of machine learning research*, *12*(7), 2121–2159.

[47] Tieleman, T. & Hinton, G. (2012). Lecture 6.5-rmsprop: Divide the gradient by a running average of its recent magnitude. *COURSERA: Neural networks for machine learning*, *4*(2), 26-30.

[48] Christaras, B. (1997). Landslides in iliolitic and marly formations. Examples from north-westem Greece. *Engineering Geology*, *47*(1-2), 57-69.

[49] Plumb, R. A. (1994). Influence of composition and texture on the failure properties of clastic rocks. In *SPE/ISRM Rock Mechanics in Petroleum Engineering* (pp. SPE-28022). SPE.

[50] Xu, B., Tan, Y., Sun, W., Ma, T., Liu, H., & Wang, D. (2023). *Study on the prediction of the uniaxial compressive strength of rock based on the SSA-XGBoost model. Sustainability 15, 5201*.

[51] Kochukrishnan, S., Krishnamurthy, P., Yuvarajan, D., & Kaliappan, N. (2024). Comprehensive study on the Python-based regression machine learning models for prediction of uniaxial compressive strength using multiple parameters in Charnockite rocks. *Scientific Reports*.

[52] Zhao, J., Li, D., Jiang, J., & Luo, P. (2024). Uniaxial Compressive Strength Prediction for Rock Material in Deep Mine Using Boosting-Based Machine Learning Methods and Optimization Algorithms. *CMES-Computer Modeling in Engineering & Sciences*, *140*(1).

[53] Daniel, C., Yin, X., Huang, X., Busari, J. A., Daniel, A. I., Yu, H., & Pan, Y. (2024). Bayesian optimization-enhanced ensemble learning for the uniaxial compressive strength prediction of natural rock and its application. *Geohazard Mechanics*, *2*(3), 197-215.

[54] Niu, L., Cui, Q., Luo, J., Huang, H., & Zhang, J. (2024). Unconfined compressive strength prediction of rock materials based on machine learning. *Journal of Engineering and Applied Science*, *71*(1), 137.

[55] Kalabarige, L. R., Sridhar, J., Subbaram, S., Prasath, P., & Gobinath, R. (2024). Machine Learning Modeling Integrating Experimental Analysis for Predicting Compressive Strength of Concrete Containing Different Industrial Byproducts. *Advances in Civil Engineering*, *2024*(1), 7844854.

[56] Yasar, E., & Erdogan, Y. (2004). Correlating sound velocity with the density, compressive strength and Young's modulus of carbonate rocks. *International Journal of Rock Mechanics and Mining Sciences*, *41*(5), 871-875.

[57] Tercan, A. E., & Ozcelik, Y. I. L. M. A. Z. (2006). Canonical ridge correlation of mechanical and engineering index properties. *International Journal of Rock Mechanics and Mining Sciences*, *43*(1), 58-65.

[58] Khanlari, G. R., Heidari, M., Momeni, A. A., & Abdilor, Y. (2012). Prediction of shear strength parameters of soils using artificial neural networks and multivariate regression methods. *Engineering Geology*, *131*, 11-18.

[59] Iyeke, S. D., Eze, E. O., Ehiorobo, J. O., & Osuji, S. O. (2016). Estimation of shear strength parameters of lateritic soils using artificial neural network. *Nigerian Journal of Technology*, *35*(2), 260-269.

[60] Mohammadi, M., Fatemi Aghda, S. M., Talkhablou, M., & Cheshomi, A. (2022). Prediction of the shear strength parameters from easily-available soil properties by means of multivariate regression and artificial neural network methods. *Geomechanics and Geoengineering*, *17*(2), 442-454.

انجمن مهندسی معدن ایران
نشریه مهندسی معدن و محیط زیست
نشانی نشریه: www.jme.shahroodut.ac.ir
دانشگاه صنعتی شاهرود

روشی برای تخمین مقاومت فشاری تک محوری (UCS) و زاویه اصطکاک داخلی (FR) با استفاده از داده‌های نگار چاه و الگوریتم‌های یادگیری عمیق

فرهاد ملائی، علی مرادزاده* و رضا محبیان

دانشکده مهندسی معدن، دانشکدگان فنی، دانشگاه تهران

اطلاعات مقاله

تاریخ ارسال: ۲۰۲۴/۰۹/۱۰
تاریخ داوری: ۲۰۲۴/۱۲/۰۴
تاریخ پذیرش: ۲۰۲۴/۱۲/۰۹

DOI: 10.22044/jme.2024.15006.2859

کلمات کلیدی

پارامترهای مکانیکی
داده‌های نگار
مدل‌های یادگیری عمیق
داده‌های مغزه
انتخاب ویژگی

چکیده

یکی از جنبه‌های مهم این مطالعه، تخمین پارامترهای مکانیکی سنگ مخزن، از جمله مقاومت فشاری محوری (UCS) و زاویه اصطکاک داخلی (FR) با استفاده از داده‌های نگار چاه است. هدف این پژوهش تخمین UCS و زاویه اصطکاک داخلی (φ) با استفاده از روش‌های جدید یادگیری عمیق شامل پرسپترون چندلایه (MLP)، حافظه کوتاه مدت بلند (LSTM)، شبکه عصبی همامیختی (CNN) و شبکه ترکیبی CNN+LSTM (CL) با استفاده از داده های نگار چاه و آزمایش مغزه یک میدان هیدروکربنی ایران است. از آنجا که تنها ۱۲ آزمایش مغزه UCS و ۶ آزمایش مغزه FR از یک چاه در این میدان در دسترس بود، ابتدا این پارامترها محاسبه و سپس به اعماق دیگر با استفاده از دو معادله جدید و نگارهای مربوطه تعمیم داده شدند. در مرحله بعد، داده‌های نگار ورودی مؤثر برای پیش‌بینی این پارامترها با روش یادگیری عمیق خود رمزگذار انتخاب شده و در نهایت مقادیر UCS و زاویه φ با استفاده از شبکه‌های MLP، LSTM، CNN و CL پیش‌بینی شدند. کارایی این چهار مدل پیش‌بینی با استفاده از مجموعه داده‌های کور و طیفی از معیارهای آماری برای داده‌های آموزشی، آزمایشی و کور ارزیابی شد. نتایج نشان می‌دهد که هر چهار مدل دقت پیش‌بینی رضایت‌بخشی دارند. با این حال، مدل CL عملکرد بهتری نسبت به سایر مدل‌ها داشت، به طوری که کمترین خطای (RMSE) برابر ۱/۰۰۵۲ و بیشترین ضریب تعیین (R^2=0.9983) برای پیش‌بینی UCS، و خطای (RMSE) مساوی ۰۲۰۱/. و ضریب تعیین برابر ۹۹۱۷/. برای پیش‌بینی زاویه φ بر روی مجموعه داده‌های کور به دست آمد.

نویسنده مسئول مکاتبات: a_moradzadeh@ut.ac.ir (ع. مرادزاده)